


Article

The Morphological Evolution of Self-Assembled Silver Nanoparticles under Photoirradiation and Their SERS Performance

Apiwat Phetsahai ¹, Pitak Eiamchai ², Kheamrutai Thamaphat ^{1,*} and Pichet Limsuwan ¹

¹ Green Synthesis and Application Laboratory, Applied Science and Engineering for Social Solution Research Unit, Department of Physics, Faculty of Science, King Mongkut's University of Technology Thonburi, Bangkok 10140, Thailand; mos_physics35@hotmail.com (A.P.); pichetlaser@gmail.com (P.L.)

² Opto-Electrochemical Sensing Research Team, National Electronics and Computer Technology Center (NECTEC), National Science and Technology Development Agency (NSTDA), Pathum Thani 12120, Thailand; pitak.eiamchai@nectec.or.th

* Correspondence: kheamrutai.tha@kmutt.ac.th; Tel.: +66-2470-8961

Abstract: In this study, we conducted a one-step photochemical synthesis to produce silver nanoparticles (AgNPs) with irregular morphology. The synthesis process involved the photoconversion of Ag nanoseeds into self-assembled Ag nanostructures of various morphologies using a high-pressure sodium lamp with a wavelength of 589 nm, corresponding to an energy of 2.1 eV. During the synthesis, the color of the colloidal Ag nanoseeds gradually changed as the irradiation time increased, transitioning from yellow to brown, juniper green, basil green, ocean green, aegean blue, and finally to true blue. We characterized the morphological evolution of the resulting AgNPs, as well as their optical properties and aggregation behavior, using transmission electron microscopy, UV-vis spectroscopy, and dynamic light scattering. Furthermore, we evaluated the impact of the self-assembled morphology of the AgNPs on their surface-enhanced Raman scattering efficiency, using R6G as the target analyte. The results revealed that the colloidal AgNPs synthesized under a visible light irradiation time of 1 h consisted of circular nanoplates, hexagonal nanoplates, trapezoid nanoplates, and triangular nanoplates. These colloidal AgNPs exhibited excellent SERS activity when used as an SERS-active substrate in the form of an aqueous solution, enabling the detection of low concentrations of R6G down to 10^{-12} M.

Keywords: silver nanoparticles; photoinduced method; Ostwald ripening; SERS; anisotropic structures



Citation: Phetsahai, A.; Eiamchai, P.; Thamaphat, K.; Limsuwan, P. The Morphological Evolution of Self-Assembled Silver Nanoparticles under Photoirradiation and Their SERS Performance. *Processes* **2023**, *11*, 2207. <https://doi.org/10.3390/pr11072207>

Academic Editors: Yew Mun Hung and Cher Pin Song

Received: 28 June 2023

Revised: 15 July 2023

Accepted: 20 July 2023

Published: 22 July 2023



Copyright: © 2023 by the authors. Licensee MDPI, Basel, Switzerland. This article is an open access article distributed under the terms and conditions of the Creative Commons Attribution (CC BY) license (<https://creativecommons.org/licenses/by/4.0/>).

1. Introduction

Over the last two decades, Raman spectroscopy (RS) has gained widespread recognition as a reliable and well-established technique for detecting and analyzing both organic and inorganic compounds in various fields, including food safety, archeology, medical diagnostics, and pharmaceuticals [1–5] due to its rapid, non-contact, and non-destructive approach. The analysis result of RS presents in the form of a Raman spectrum, which exhibits multiple peaks with varying positions and relative intensities. The position of Raman peaks typically provides molecular fingerprint information regarding vibrational and rotational molecular modes, representing the molecular composition of the analyte. Meanwhile, the intensity of Raman peaks is employed for quantitative analysis. Nevertheless, RS has some limitations, including its lower efficiency in capturing inelastic light scattering compared to elastic scattering, which hampers its ability to detect low analyte concentrations. Additionally, a strong fluorescence background poses another challenge [6,7]. To overcome these problems, surface-enhanced Raman scattering (SERS) is employed to enhance the Raman signal intensity and to quench fluorescence, thereby improving the signal-to-noise ratio.

SERS involves an increase in the inelastic light scattering of analytes that are either adsorbed onto or located near the surface of noble metal nanostructures. Two main mechanisms contribute to this amplified inelastic light scattering: electromagnetic (EM) enhancement, which arises from the local electric fields induced near metallic surfaces, and chemical enhancement, which is attributed to the charge transfer interaction between the analyte molecule and the metallic surface [8–13]. EM enhancement plays a significant role in the SERS phenomenon, particularly in situations wherein the molecule is located within the narrow gap between closely spaced nanostructures [9]. In brief, when incident light irradiates the metal nanostructures, the collective oscillation of electrons within them induces a plasma resonance, accompanied by a significant increase in the light-induced electric field strength inside and around the metal nanostructures. The analyte molecules adsorbed onto or near the surface of metal nanostructures are stimulated by the combined effects of the original incident and induced electric fields, resulting in the amplification of Raman signal intensity. Metal nanostructures serve as platforms to enhance the inelastic light scattering of analyte molecules, and are widely recognized as SERS-active substrates.

Up to now, many forms of SERS-active substrates have been developed and can be classified into two main groups: liquid colloidal substrates, consisting of metallic nanoparticles (NPs) suspended in a solution, and solid substrates comprising periodic ordered arrays of metallic nanostructures deposited on a flat surface [14–17]. The use of colloidal SERS-active substrates is widespread due to their easy preparation and handling. Among various types of noble metal nanoparticles, silver (Ag), gold (Au), and copper (Cu) NPs exhibit strong localized surface plasmon resonance (LSPR) in the visible and near-infrared region due to their unique optical properties. However, AgNPs, in particular, provide the highest SERS intensities due to their interband transitions found in the ultraviolet range, resulting in minimal absorption in the visible or near-infrared Raman wavelengths [6,18,19]. The LSPR response of AgNPs exhibits a distinct dependence on their morphology, particularly with regard to their size and shape [6,8,11,18–20]. Moreover, the distance between adjacent AgNPs, which influences the generation of intense local electric fields referred to as hot spots, also exerts a significant impact on SERS enhancement [10,15,21,22]. Consequently, the controllable size and shape of AgNPs have garnered considerable attention due to their ability to enhance SERS activity.

Many researchers have dedicated their efforts to synthesize AgNPs with highly curved surfaces and sharp features, such as triangular nanoplates, hexagonal nanoplates, and quasi-spherical shapes, aiming to explore their potential in SERS measurements. Mostly, each specific shape and size of AgNPs has been synthesized using a photochemical method, wherein a nanoseed dispersion is transformed into different shapes by exposure to specific light sources such as sunlight, UV light, or visible light, depending on the desired shape [15,18,19,21,23–27]. However, to date, no studies have investigated the morphology-dependent SERS performance of AgNPs synthesized using a one-step synthesis method for driving the growth and formation of different AgNPs morphologies throughout the entire process.

In this study, we present an alternative approach to synthesizing AgNPs with diverse morphologies, and examine their impact on SERS activity, which distinguishes our research from previous works in this field. The various shapes of colloidal AgNPs were self-assembled from spherical nanoseeds through photoconversion using a single light source, specifically a high-pressure sodium lamp. The resulting nanoparticles were subsequently characterized in terms of their optical and physical properties, and their agglomeration tendencies. The as-prepared AgNPs obtained at different light exposure times were utilized as a colloidal SERS-active substrate in the form of an aqueous solution, without the need for paste drop-casting. This approach enabled the differentiation of plasmon coupling from particle aggregation and plasmon resonance effects [23]. The influence of the self-assembled AgNPs' morphology on SERS efficiency was evaluated using rhodamine 6G (R6G) as the target analyte.

2. Materials and Methods

2.1. Synthesis of Spherical Ag Nanoseeds

In order to synthesize AgNPs with varying shapes and sizes using the photochemical method, Ag nanoseeds were employed as the initial building blocks. Colloidal solutions containing spherical Ag nanoseeds were prepared following a conventional chemical reduction method with a customized recipe, as described below. The chemical reagents used in this study, including silver nitrate (AgNO_3), trisodium citrate ($\text{Na}_3\text{C}_6\text{H}_5\text{O}_7$), and sodium borohydride (NaBH_4) were obtained from the following suppliers: AgNO_3 from POCH (Gliwice, Poland), $\text{Na}_3\text{C}_6\text{H}_5\text{O}_7$ from Ajax Finechem (Cherrybrook, NSW, Australia), and NaBH_4 from QReC (Asia) Sdn. Bhd. (Kuala Lumpur, Malaysia). For the synthesis, 0.75 mL of a 10 mM AgNO_3 solution and 0.75 mL of a 10 mM $\text{Na}_3\text{C}_6\text{H}_5\text{O}_7$ solution were added to 72 mL of deionized water. The mixture was stirred at a rate of 433 rpm for 30 min. Subsequently, 37.5 μL of an 8 mM NaBH_4 solution was slowly added dropwise to the mixture, and stirring was continued for an additional 2 min. To allow for further development, the resulting solution was aged at 4 °C in the dark for 2 h before being used as a seed.

2.2. Synthesis of Self-Assembled AgNPs with Varying Morphologies

In this step, 20 mL of colloidal spherical Ag nanoseeds were transferred into a glass vial and exposed to visible light irradiation at a wavelength of 589 nm for the photoconversion process. Two high-pressure sodium lamps (Luna, SC735, Bangkok, Thailand) were employed as the light source to facilitate the self-assembly process of AgNPs with diverse shapes. The photo-transformation was carried out under an irradiance of approximately 130 mW/cm^2 , measured using a digital power meter (Thorlabs, Inc., PM120D, Newton, NJ, USA), at a temperature of 39.1 ± 0.6 °C. To protect the colloidal solution from unnecessary irradiation, the vial was positioned between two high-pressure sodium lamps at a distance of 13 cm from the lamp surfaces, within an opaque box, as illustrated in Figure 1. The duration of irradiation was varied over different time intervals: 15 min, 30 min, 1 h, 2 h, 3 h, 4 h, and 5 h. Additionally, colloidal spherical Ag nanoseeds without light irradiation were also observed as a control to confirm the influence of light on shape conversion. Throughout the process, the morphological evolution and agglomeration of the synthesized AgNPs were carefully monitored and analyzed.

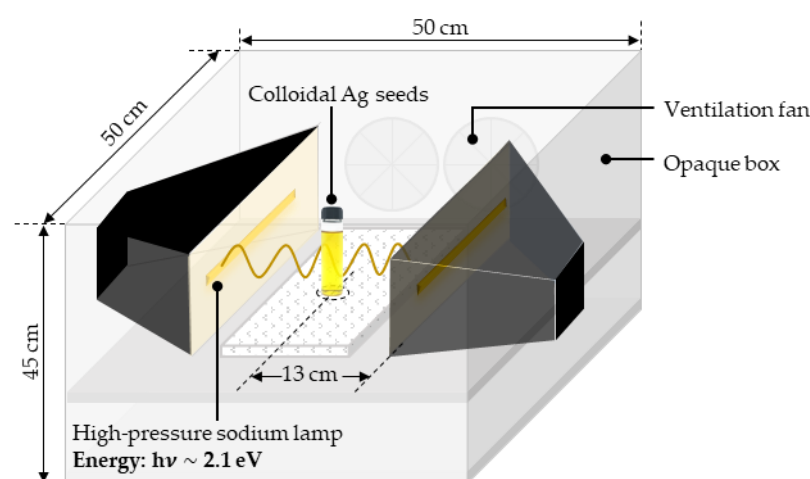


Figure 1. Schematic illustration of the experimental setup for the photoconversion of Ag nanoseeds into different morphologies.

2.3. Characterization Methods

The optical properties of the colloidal Ag nanoseeds and the photoinduced AgNPs were analyzed using a UV-visible spectrometer (Avantes, AvaSpec-EDU, Bangkok, Thai-

land) with a measurement range of 350–850 nm. The morphology and particle size were monitored using a transmission electron microscope (TEM; Hitachi High-Tech Corporation, HT7800, Tokyo, Japan) operating at an acceleration voltage of 120 kV. Additionally, the zeta potential, which provides information about the surface charge of the nanoparticles, was measured using dynamic light scattering (DLS) with a Zetasizer (Malvern Panalytical plc, Nano ZS, Malvern, Worcs, UK).

2.4. Design of Sample Holder for SERS Measurement

In order to reduce any undesired effects arising from drop casting, enhance stability and reproducibility, improve sensitivity, and enable real-time monitoring, SERS measurements were conducted using aqueous solutions without the use of drop casting. To facilitate the analysis, a custom-designed sample holder was developed to securely hold solution samples during SERS measurements. This design aimed to ensure optimal interaction between the colloidal SERS-active substrate and the analyte molecules.

A cost-effective liquid chamber with dimensions of $3 \times 5 \times 5 \text{ mm}^3$ was fabricated using 3D printing technology to precisely match the required dimensions. This chamber, as shown in Figure 2, was securely mounted onto a glass slide covered with aluminum foil, which served as a reflective surface to enhance the detection of SERS signals. It was employed as a sample holder for SERS measurement.

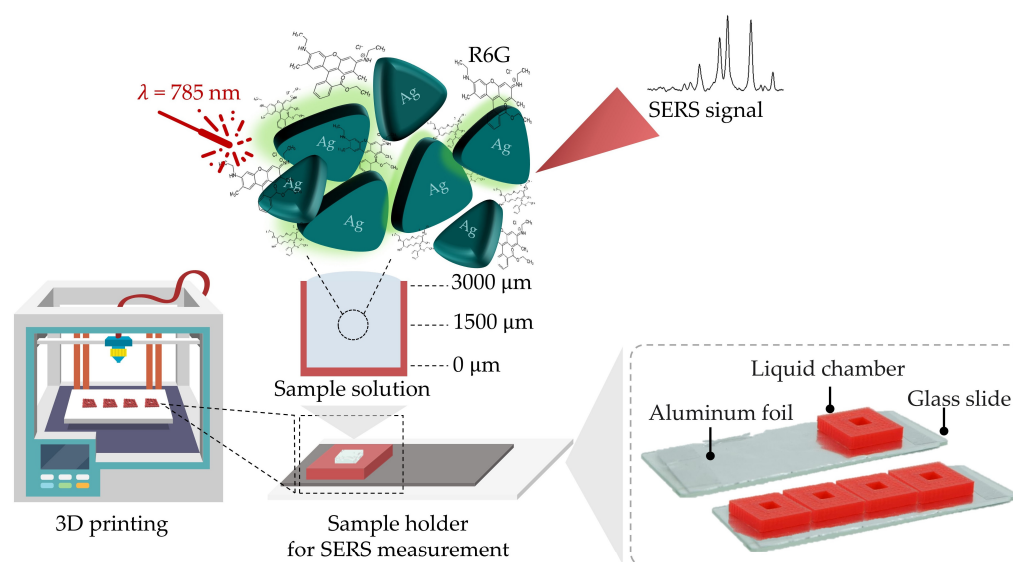


Figure 2. Schematic of sample holder preparation for Raman measurement.

2.5. SERS Experimental Details

The SERS performance of a colloid solution consisting of self-assembled AgNPs was investigated using R6G as the testing analyte. After synthesizing colloidal AgNPs at each irradiation time, 200 μL of the resulting solution was collected. Subsequently, it was mixed thoroughly with a 200 μL solution of 10^{-4} M R6G (dye content 99%, Sigma-Aldrich, Bangkok, Thailand) using a vortex mixing method for 10 s to ensure homogeneity. To explore the optimal conditions for AgNP synthesis, the photochemically synthesized AgNP solution prepared at different irradiation times was mixed with the R6G at a concentration of 10^{-4} M. To investigate the highest SERS performance, the selected AgNP solution prepared at the best irradiation time was mixed with an R6G solution ranging from 10^{-4} to 10^{-12} M.

For SERS characterization, 200 μL of the resulting mixture was transferred to a liquid chamber and subjected to Raman spectrometry analysis. The Raman spectra were recorded using a Raman spectrometer (Renishaw plc., inVia, Wotton-under-Edge, Glos, UK) with an excitation wavelength of 785 nm and a maximum output power of 20 mW. The laser beam was focused on the middle height of the chamber using a $50\times$ objective lens.

Each measurement was recorded at a single point with a 10 s acquisition time and three accumulations. The Raman enhancement factor was calculated, and the colloidal AgNPs synthesized under specific irradiation time that provided the highest SERS performance were further investigated for their ability to detect R6G in a dilution series.

It is important to emphasize that these experimental details were consistently applied in all SERS measurements conducted throughout the study, ensuring the comparability and validity of the obtained results.

3. Results and Discussion

3.1. Formation of Spherical Ag Nanoseeds

The formation of Ag nanoseeds involves the reduction of a silver precursor in the presence of a reducing agent and a stabilizing agent. In this work, silver nitrate served as a reducing agent, facilitating the reduction of Ag^+ to form AgNPs.

As seen in Figure 3, sodium borohydride reduced Ag^+ to silver atoms (Ag^0), which served as nucleation sites for nanoparticle formation. Trisodium citrate subsequently interacted with Ag^0 , facilitating the formation of small Ag nanoseeds [21]. The resulting small Ag nanoseeds, with a diameter of 2–6 nm, acted as both a catalyst for the oxidation of sodium borohydride and a template for the deposition of additional Ag^0 , leading to the formation of larger Ag nanoseeds with a diameter of 6–10 nm [21,28,29].

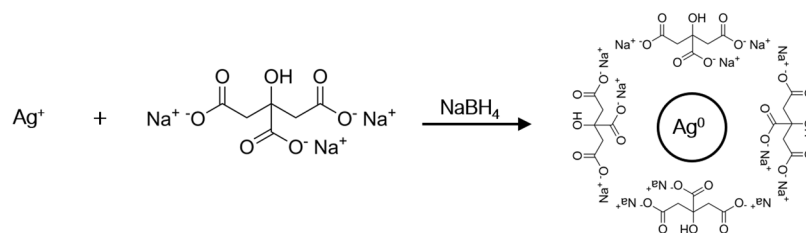


Figure 3. Diagram pathway of Ag nanoseeds' formation.

Figure 4a shows the UV-vis absorption spectrum of the synthesized Ag nanoseeds solution, displaying a yellow color. The spectrum exhibited a distinct peak around 397 nm, indicating the presence of the dipole plasmon absorption of the spherical AgNPs [30,31]. This observation was consistent with the TEM result presented in Figure 4b, which showed that the synthesized Ag nanoseeds were spherical in shape, with a diameter below 10 nm. The nanoseeds consisted of small and large nanoseeds with diameters of 2.9 ± 0.2 nm and 6.6 ± 0.4 nm, respectively.

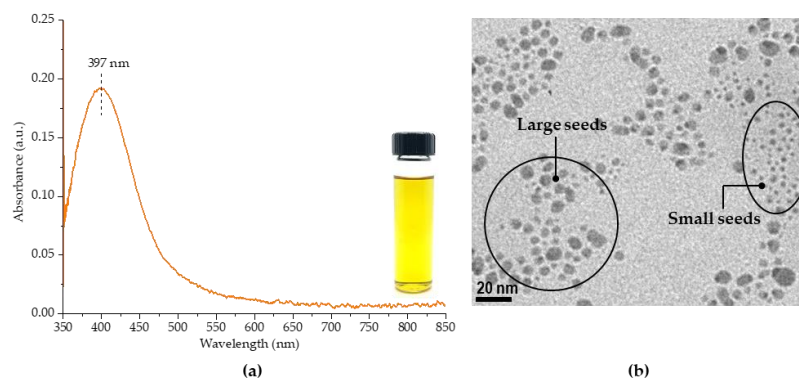


Figure 4. (a) UV-vis absorption spectrum and (b) TEM image of the synthesized Ag nanoseeds.

3.2. Morphological Evolution of Photoinduced AgNPs

In photomediated synthesis, the Ag nanoseeds synthesized in the previous section were exposed to visible light irradiation at a wavelength of 589 nm (energy = 2.1 eV) for varying durations ranging from 15 min to 5 h. Additionally, the Ag nanoseeds were kept

in the dark for the same duration without irradiation to investigate the effect of light irradiation in the photoconversion process.

The results revealed that in the absence of light irradiation, the solution maintained a consistent light-yellow color, and the absorption spectra exhibited a distinct peak around 397 nm, as illustrated in Figure 5. However, with longer incubation times, there was a slight increase in the absorption intensity, suggesting a corresponding increase in the number of nanoseeds [32]. This confirmed that there was no transformation of spherical nanoseeds into other shapes. In contrast, when the Ag nanoseeds were subjected to irradiation, a noticeable color change occurred. As shown in Figure 6, as the irradiation time increased, a gradual change in the color of the Ag nanoseeds was observed, ranging from a light yellow hue to shades of brown, juniper green, basil green, ocean green, aegean blue, and finally, true blue. These distinct colors were attributed to the surface plasmon resonance (SPR) effect, indicating a change in the geometry of AgNPs [21,30]. These findings demonstrate the significant influence of light irradiation on the photoconversion process, leading to the observed color changes and potential shape transformations of the Ag nanoseeds.

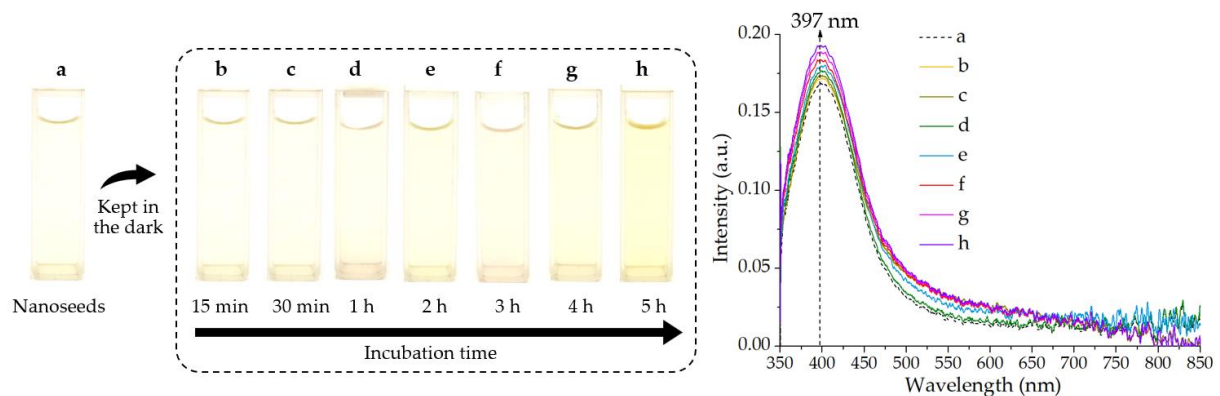


Figure 5. Digital images of the Ag nanoseeds at different incubation times without light irradiation, along with the corresponding time evolution of UV-vis absorption spectra: (a) nanoseeds, (b) 15 min in the dark, (c) 30 min in the dark, (d) 1 h in the dark, (e) 2 h in the dark, (f) 3 h in the dark, (g) 4 h in the dark, and (h) 5 h in the dark.

To examine the morphological evolution and corresponding optical properties of the Ag nanostructure, UV-vis spectroscopy and TEM measurements at various irradiation times (15 min, 30 min, 1 h, 2 h, 3 h, 4 h, and 5 h) were conducted. These analyses enabled us to investigate the structural changes, confirm the presence of different nanoparticle shapes at different irradiation times, and provide additional evidence of the photoinduced modifications in the synthesized nanoparticles.

Upon examining the UV-vis spectra in Figure 6, we observed that the Ag nanoseeds irradiated for 15 min exhibited a redshift of the original peak at 397 nm, which was characteristic of spherical seeds, to approximately 440 nm, with increased intensity. This redshift was attributed to the growing contribution of higher-order plasmon modes, as predicted by Mie theory [30]. The observed redshift indicated the transformation of Ag nanoseeds into larger-sized spherical AgNPs with higher particle concentrations [23,33]. As the irradiation time reached 30 min, the band at 440 nm shifted further to 450 nm with a gradual increase in intensity. Additionally, a new broad band around 660 nm, attributed to the in-plane dipole plasmon resonance, emerged with an absorbance intensity less than twice that of the 450 nm wavelengths. This spectral feature suggested the growth of spherical AgNPs into larger particles, and the transformation of some particles into circular nanoplates [34].

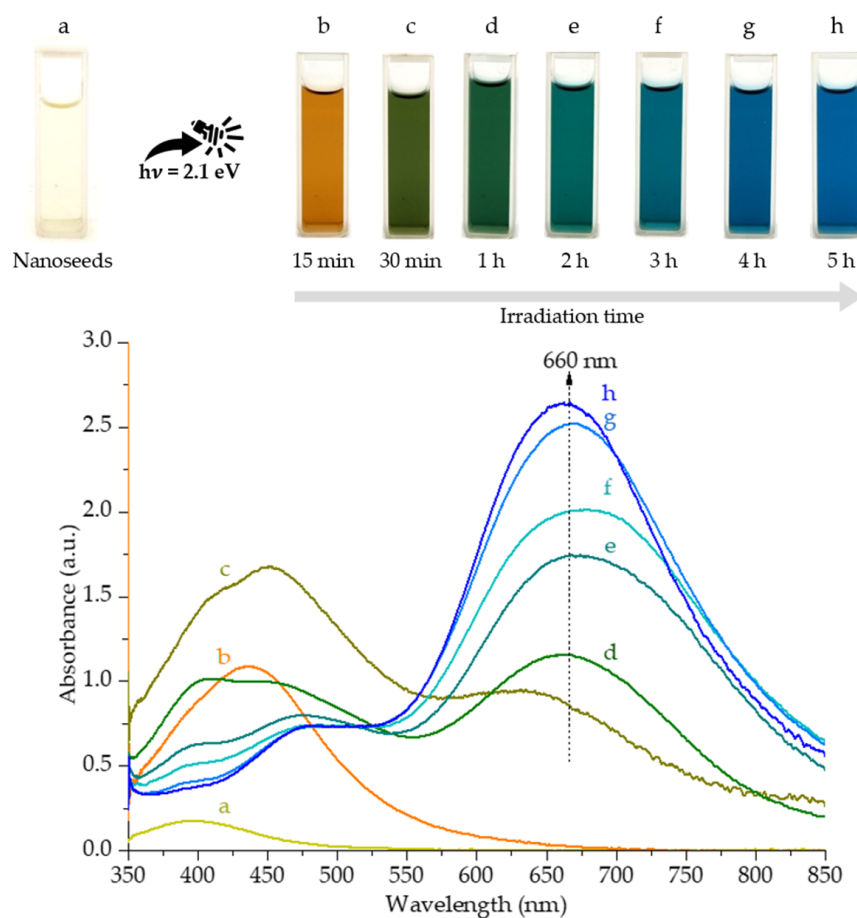


Figure 6. Digital images and UV-vis absorption spectra depict the color change and time evolution of Ag nanoseeds under different irradiation times: (a) nanoseeds, (b) 15 min, (c) 30 min, (d) 1 h, (e) 2 h, (f) 3 h, (g) 4 h, and (h) 5 h.

At an irradiation time of 1 h, the intensity of the 450 nm band decreased and split into two broad bands with maximum intensity at 400 nm and 475 nm, while the band at 660 nm became more prominent. The bands at 400 nm and 475 nm were attributed to the out-of-plane dipole plasmon resonance, while the bands at 660 nm were associated with in-plane dipole plasmon resonance [34]. These absorption peaks indicated the shape transformation of AgNPs from circular nanoplates to triangular nanoplates. However, given the relatively short irradiation time of approximately 1 h, the shape of the AgNPs was in a transitional stage, potentially resulting in multi-shaped nanoplates, such as circular nanoplates, hexagonal nanoplates, trapezoid nanoplates, and truncated triangular nanoplates [25]. As the irradiation time exceeded 1 h, the small broad peak around 400 nm diminished, while the maximum peak around 660 nm continued to significantly increase due to the formation of more triangular nanoplates [30,35]. These observations demonstrated that the Ag nanoseeds underwent growth into anisotropic AgNPs with diverse geometries, and the extent of this transformation was found to be dependent on the irradiation time. The TEM images in Figure 7 provide visual confirmation of these findings.

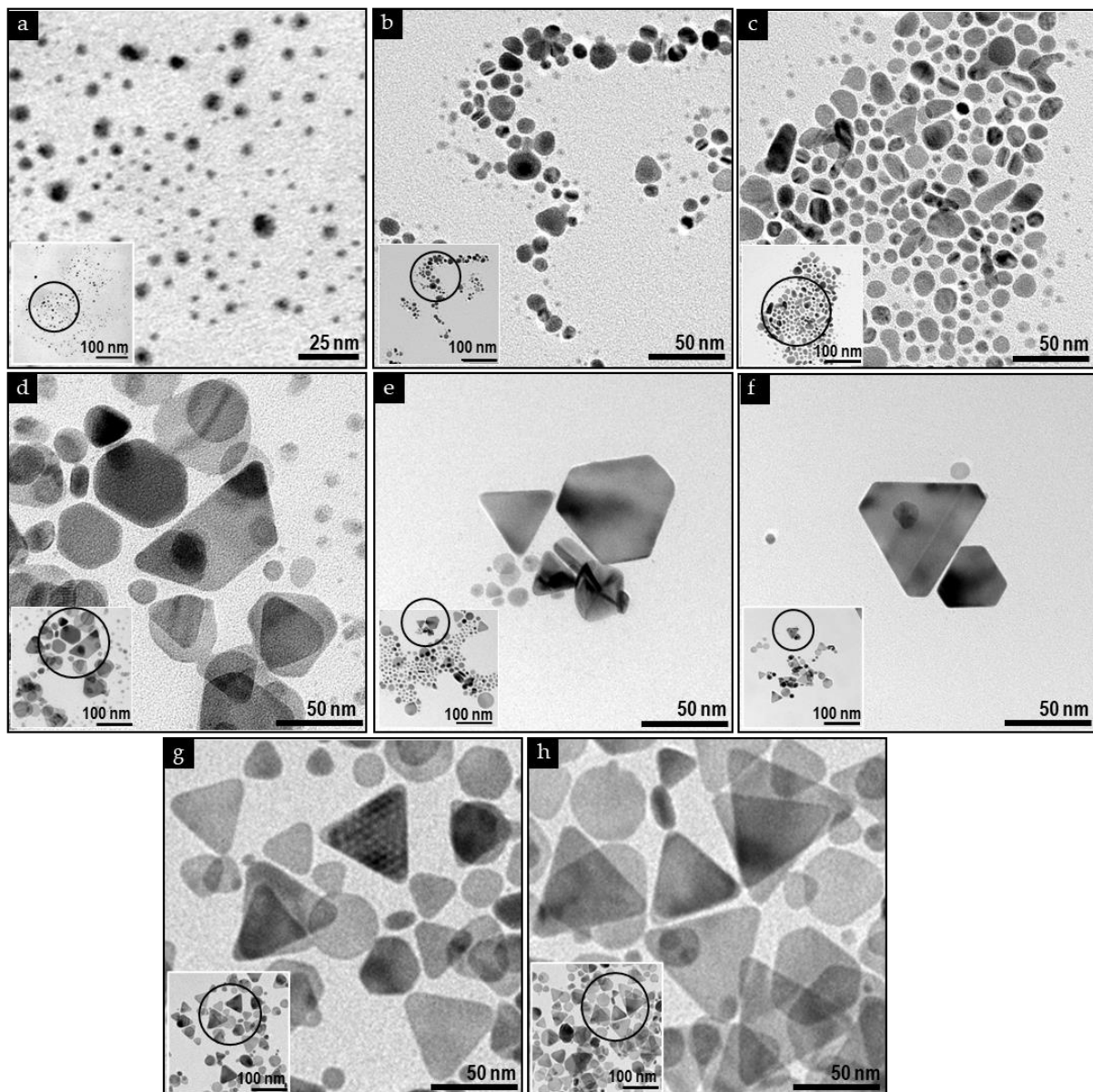







Figure 7. TEM images illustrating the morphology of Ag nanoseeds under different irradiation times: (a) nanoseeds, (b) 15 min, (c) 30 min, (d) 1 h, (e) 2 h, (f) 3 h, (g) 4 h, and (h) 5 h. Insets highlight specific areas magnified in the highest resolution image.

Figure 7 shows TEM images illustrating the presence of small and large nanoseeds in the Ag sample prior to irradiation, with an overall size of 3.1 ± 0.1 nm. After 15 min of irradiation, these nanoseeds grew into larger nanoparticles with an approximate diameter of 12.5 ± 0.2 nm. Subsequently, at 30 min of irradiation, some of these nanoparticles started to assemble into circular nanoplates, exhibiting a diameter of 18.7 ± 1.6 nm.

At an irradiation time of 1 h, the AgNPs exhibited a variety of highly anisotropic structures, including circular nanoplates with an average diameter of 19.3 ± 1.5 nm, hexagonal nanoplates with an average edge length of 30.7 ± 1.9 nm, trapezoid nanoplates with an average edge length of 16.0 ± 1.3 nm, and truncated triangular nanoplates with an average edge length of 27.2 ± 2.1 nm. Furthermore, as the irradiation time exceeded 1 h, an increased number of triangular nanoplates were observed, and their average size also increased with longer irradiation periods. The morphology evolution observed throughout the photoconversion process at different irradiation times is summarized in Table 1,

and Figure 8 exemplifies the morphology transformation of spherical NPs into triangular nanoplates during the photoconversion process.

Table 1. The morphology, average size, and percentage population of AgNPs synthesized under visible light irradiation at a wavelength of 589 nm.

Irradiation Time		Morphology				
		Spherical Nanoparticle	Circular Nanoplate	Hexagonal Nanoplate	Trapezoid Nanoplate	Triangular Nanoplate
						
Seed (0 min)	Average size Population	3.1 ± 0.1 nm 100%	- -	- -	- -	- -
15 min	Average size Population	12.5 ± 0.2 nm 100%	- -	- -	- -	- -
30 min	Average size Population	15.1 ± 0.6 nm 82%	18.7 ± 1.6 nm 18%	- -	- -	- -
1 h	Average size Population	- -	19.3 ± 1.5 nm 46%	30.7 ± 1.9 nm 12%	16.0 ± 1.3 nm 10%	27.2 ± 2.1 nm 32%
2 h	Average size Population	- -	24.6 ± 1.1 nm 47%	36.1 ± 1.6 nm 7%	35.5 ± 1.0 nm 11%	30.5 ± 2.6 nm 35%
3 h	Average size Population	- -	24.7 ± 1.1 nm 40%	37.9 ± 3.4 nm 6%	- -	34.2 ± 1.1 nm 54%
4 h	Average size Population	- -	28.2 ± 1.0 nm 39%	32.5 ± 4.3 nm 3%	- -	36.2 ± 1.1 nm 58%
5 h	Average size Population	- -	29.9 ± 1.0 nm 34%	44.3 ± 4.5 nm 4%	- -	41.1 ± 1.2 nm 62%

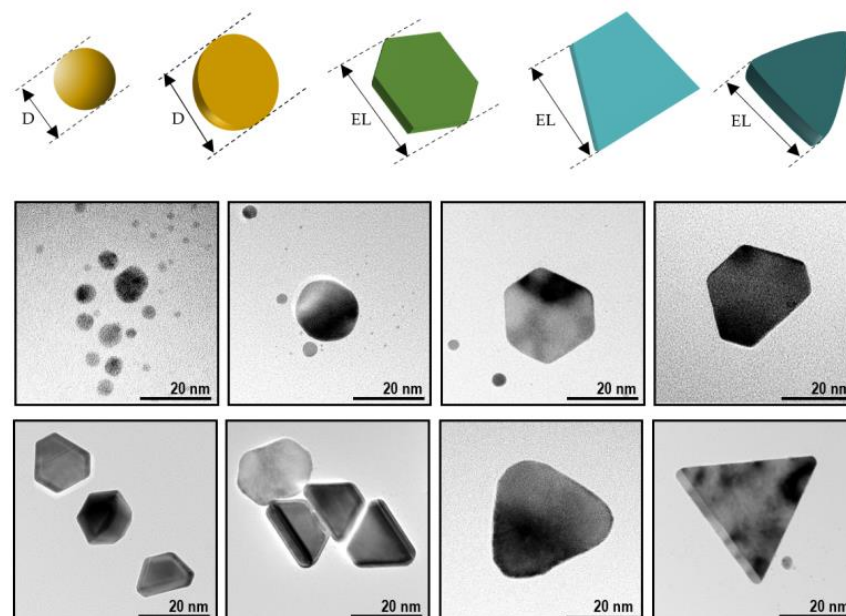


Figure 8. TEM images of the morphology transformation of spherical AgNPs into triangular Ag nanoplates during the photoconversion process at a wavelength of 589 nm (D represents the diameter, and EL represents the edge length).

The phenomenon governing the photoconversion of Ag nanoseeds into irregular-shaped AgNPs is known as Ostwald ripening [19,30]. In this process, Ag^+ was initially induced by sodium borohydride into Ag nanoseeds. Simultaneously, citrate ions produced

electrons that participated in the reduction of Ag^+ under light irradiation. Subsequently, the nanoseeds bonded with Ag^+ to create dimer Ag_2^+ , which interacted with citrate ion due to affinity, resulting in growth along the (111) plane and ultimately leading to the formation of triangular-shaped nanoparticles [24,25,36,37].

For the analysis of nanoparticle aggregation, valuable insights were obtained through the measurement of zeta potential (ξ) values using a Zetasizer. It was found that the ξ values of the colloidal Ag nanoseeds and the colloidal AgNPs obtained after irradiation for 15 min, 30 min, 1 h, 2 h, 3 h, 4 h, and 5 h were -30.93 , -35.57 , -36.37 , -26.77 , -29.40 , -29.90 , -31.70 , and -34.39 mV, respectively. These results indicated that the AgNPs obtained after 1 h of irradiation occupied the highest degree of aggregation [38].

3.3. The Effect of Morphology on SERS Efficiency

The Ag nanoseeds (without light irradiation) and self-assembled AgNPs synthesized under visible light irradiation at a wavelength of 589 nm (energy = 2.1 eV) were utilized as the SERS-active substrate in an aqueous solution without the need for drop casting. For this study, a custom sample holder, as shown in Figure 2, was exclusively employed to detect R6G using an excitation wavelength of 785 nm. The Raman band assignments related to R6G are summarized in Table 2.

Table 2. Assignment of Raman bands in the SERS spectra of R6G.

Raman Shift (cm^{-1})	Band Assignments	References
772 (w)	C-H out-of-plane bending	[39–41]
1087 (w)	-	[40–42]
1125 (w)	C-H in-plane bending in xanthene/phenyl rings	[40,41]
1182 (m)	C-H in-plane bending in xanthene rings	[41]
1311 (w)	Hybrid mode (xanthene/phenyl rings and NHC_2H_5 group)	[41]
1363 (s)	C–C stretching in xanthene ring	[40,41]
1511 (s)	C–C stretching in xanthene ring	[40,41]
1575 (s)	C–C stretching in phenyl ring	[40,41]
1648 (s)	C=C stretching in xanthene ring	[39–42]

Abbreviations: s = strong peak intensity, m = middle peak intensity, and w = weak peak intensity.

Figure 9a presents the SERS efficiency of all substrates for the detection of the R6G molecules with a concentration of 10^{-4} M. It is evident that the characteristic Raman bands of R6G were too weak to be observed in the absence of an SERS substrate (normal Raman), including the use of colloidal Ag nanoseeds without irradiation. However, when colloidal AgNPs synthesized under a 30 min irradiation time were used as the SERS substrate, the Raman signal of R6G became easily detectable. Notably, the Raman signal intensities of a strong primary peak at 1363 cm^{-1} , corresponding to the C-C ring stretching vibration, were observed (Figure 9b). These intensities were utilized to calculate the estimated enhancement factor (EF) by comparing the SERS spectrum intensity (I_{SERS}) with the normal Raman intensity (I_{Raman}) [23,43].

Upon analyzing the calculated EF values presented in Table 3, a notable trend emerged. The EF value demonstrated a rapid increase, reaching its peak at 1961 when utilizing colloidal AgNPs synthesized under irradiation for a duration of 1 h as the SERS-active substrate. Following this, a slight decrease was observed, with the EF value registering at 1720 when colloidal AgNPs synthesized under a 2 h irradiation time were used as the SERS-active substrate. Subsequently, a sudden and significant decrease in the EF value was observed. These results indicated that colloidal AgNPs, composed of mixed shapes including circular nanoplates, hexagonal nanoplates, trapezoid nanoplates, and triangular nanoplates, exhibited a higher EF value compared to other conditions.

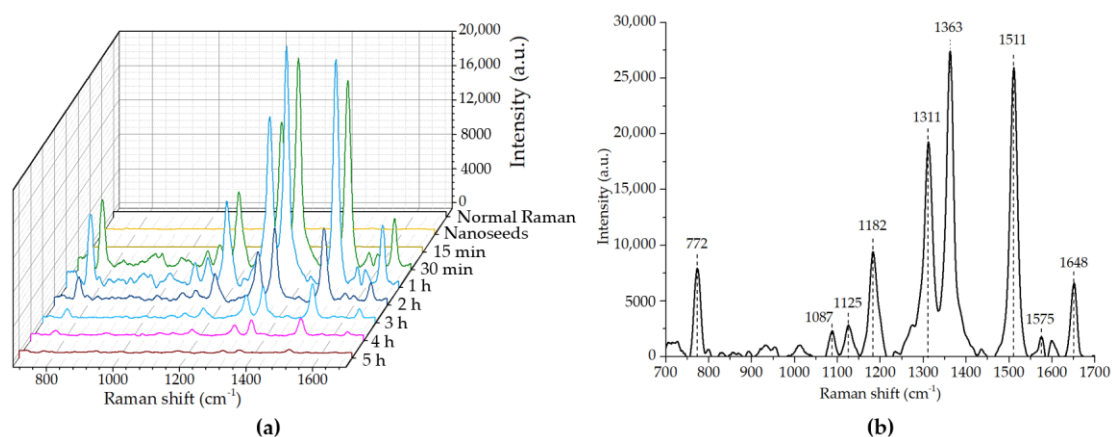


Figure 9. (a) Evolution of SERS spectral results as measured from the solution of the AgNPs, photochemically irradiated at 15 min to 5 h, and mixed with 10^{-4} M R6G analyte solution. For reference, the figure includes Raman spectra of the non-irradiated Ag nanoseeds and the 10^{-4} M R6G solution, respectively. (b) The Raman peak assignment of the SERS-active AgNPs solution, irradiated for 1 h and mixed with the 10^{-4} M R6G solution.

Table 3. Raman enhancement factor of 10^{-4} M R6G on colloidal SERS-active substrates synthesized under different irradiation times.

Irradiation Time	AgNPs Morphology	EF at 1363 cm^{-1} (times) EF $\sim [I_{\text{SERS}}]/[I_{\text{Raman}}]$
15 min		2
30 min		601
1 h		1961
2 h		1720
3 h		257
4 h		205
5 h		126

The presence of triangular nanoplates with appropriate edge lengths, which possess a high anisotropic structure, was identified as a key feature contributing to the colloidal AgNPs synthesized under an hour irradiation time exhibiting the highest SERS activity [6]. This was partly due to R6G molecules easily bonding with the abundant (111) faces of nanoplates [18,23]. In addition, the nanoplates exhibited dipolar vibrations, including dipolar out-of-plane vibrations observed at 400 nm and 475 nm, as well as dipolar in-plane vibrations observed at 660 nm. These vibrations facilitated efficient energy transfer between the incident light and the nanoplates, further enhancing the Raman scattering signal [44]. Furthermore, the highest degree of particle aggregation of colloidal AgNPs irradiated for 1 h (ξ values = -26.67 mV) resulted in the formation of hotspots, which also contributed to the observed enhancement in the Raman scattering signal.

Then, the colloidal AgNPs synthesized under an irradiation time of 1 h were used to evaluate the SERS performance with different concentrations of R6G ranging from 10^{-12} to 10^{-4} M. The spectral results, depicted in Figure 10, demonstrated the remarkable capability of the AgNPs synthesized under the 1 h irradiation time to significantly enhance the Raman signal of R6G, even at low concentrations as low as 10^{-12} M. Furthermore, a clear linear correlation was observed between the concentration of R6G and the strong Raman peak intensities at 1363 and 1511 cm^{-1} , as illustrated in Figure 11. The obtained

linear correlation, with a high correlation coefficient (R^2) exceeding 0.99, underscored the reliability and robustness of the SERS measurements. This signified that the SERS technique utilizing the AgNPs synthesized under the 1 h irradiation time could provide precise and accurate quantitative measurements of R6G concentrations.

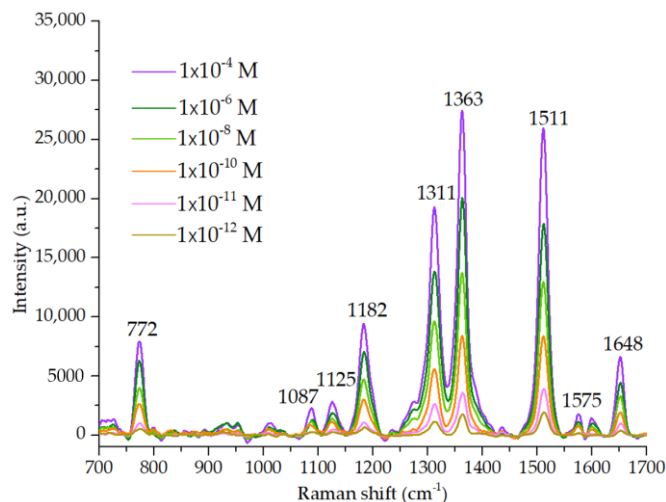


Figure 10. SERS spectra of the mixed solution of the AgNPs, irradiated at 1 h and prepared with the R6G analyte solution at different concentrations: 10^{-12} , 10^{-11} , 10^{-10} , 10^{-8} , 10^{-6} , and 10^{-4} .

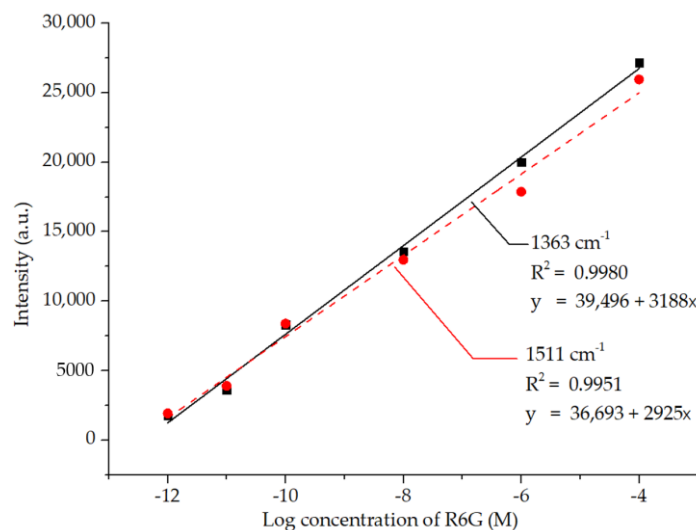


Figure 11. Calibration curves of SERS intensity for the strong peaks at 1363 and 1511 cm^{-1} .

4. Conclusions

In this research, we have successfully developed self-assembled Ag nanostructures of different morphologies, including circular nanoplates, hexagonal nanoplates, trapezoid nanoplates, and triangular nanoplates, using a one-step photosynthesis method. The Ag nanoseeds, consisting of small and large nanoparticles with a diameter of less than 10 nm, were photoconverted into different morphologies of AgNPs by employing a simple and affordable high-pressure sodium lamp with a wavelength of 589 nm, corresponding to an energy of 2.1 eV. Furthermore, this research provides valuable insights into the morphology evolution of synthesized AgNPs and their impact on SERS performance. The SERS efficiency of the AgNPs depended on factors such as shape, size, and particle aggregation. The knowledge gained from this research can guide the detection of target molecules in trace compound analysis and sensing, using an SERS-active substrate in the form of an aqueous solution. This approach eliminated the need for complicated methods,

such as drop casting, which require a waiting time for substrate drying, and managed to avoid the coffee ring effect.

Author Contributions: Conceptualization, A.P., K.T. and P.E.; methodology, A.P. and K.T.; software, A.P.; validation, A.P., K.T., P.E. and P.L.; investigation, A.P.; resources, K.T.; data curation, A.P.; writing—original draft preparation, A.P. and K.T.; writing—review and editing, K.T. and P.L.; supervision, P.E. and P.L.; project administration, A.P.; funding acquisition, A.P., K.T. and P.L. All authors have read and agreed to the published version of the manuscript.

Funding: This research was funded by the Faculty of Science, King Mongkut's University of Technology Thonburi, the Science Achievement Scholarship of Thailand, and the National Research Council of Thailand (NRCT).

Data Availability Statement: Data sharing not applicable.

Acknowledgments: The authors would like to thank the National Science and Technology Development Agency for providing the Raman spectrometer.

Conflicts of Interest: The authors declare no conflict of interest.

References

1. Zhao, L.; Gu, W.; Zhang, C.; Shi, X.; Xian, Y. In Situ Regulation Nanoarchitecture of Au Nanoparticles/Reduced Graphene Oxide Colloid for Sensitive and Selective SERS Detection of Lead Ions. *J. Colloid Interface Sci.* **2016**, *465*, 279–285. [[CrossRef](#)] [[PubMed](#)]
2. Paudel, A.; Rajjada, D.; Rantanen, J. Raman Spectroscopy in Pharmaceutical Product Design. *Adv. Drug Deliv. Rev.* **2015**, *89*, 3–20. [[CrossRef](#)]
3. Bersani, D.; Conti, C.; Matousek, P.; Pozzid, F.; Vandenabeele, P. Methodological Evolutions of Raman Spectroscopy in Art and Archaeology. *Anal. Methods* **2016**, *8*, 8395–8409. [[CrossRef](#)]
4. Li, L.; Cao, X.; Zhang, T.; Wu, Q.; Xiang, P.; Shen, C.; Zou, L.; Li, Q. Recent Developments in Surface-Enhanced Raman Spectroscopy and Its Application in Food Analysis: Alcoholic Beverages as an Example. *Foods* **2022**, *11*, 2165. [[CrossRef](#)]
5. Kong, K.; Kendall, C.; Stone, N.; Notingham, I. Raman Spectroscopy for Medical Diagnostics—From In-Vitro Biofluid Assays to In-Vivo Cancer Detection. *Adv. Drug Deliv. Rev.* **2015**, *89*, 121–134. [[CrossRef](#)]
6. Zannotti, M.; Rossi, A.; Giovannetti, R. SERS Activity of Silver Nanosphere, Triangular Nanoplates, Hexagonal Nanoplates and Quasi-Spherical Nanoparticles: Effect of Shape and Morphology. *Coatings* **2020**, *10*, 288. [[CrossRef](#)]
7. Ramirez-Perez, J.C.; Reis, T.A.; Olivera, C.L.P.; Rizzutto, M.A. Impact of Silver Nanoparticles Size on SERS for Detection and Identification of Filamentous Fungi. *Spectrochim. Acta A Mol. Biomol. Spectrosc.* **2022**, *272*, 120980. [[CrossRef](#)] [[PubMed](#)]
8. Israelsen, N.D.; Hanson, C.; Vargis, E. Nanoparticle Properties and Synthesis Effects on Surface-Enhanced Raman Scattering Enhancement Factor: An Introduction. *Sci. World J.* **2015**, *2015*, 124582. [[CrossRef](#)]
9. Pustovit, V.N.; Shahbazyan, T.V. Quantum-Size Effects in SERS from Noble-Metal Nanoparticles. *Microelectron. J.* **2005**, *36*, 559–563. [[CrossRef](#)]
10. Petryayeva, E.; Krull, U.J. Localized Surface Plasmon Resonance: Nanostructures, Bioassays and Biosensing—A review. *Anal. Chim. Acta* **2011**, *706*, 8–24. [[CrossRef](#)]
11. Rycenga, M.; Camargo, P.H.C.; Li, W.; Moran, C.H.; Xia, Y. Understanding the SERS Effects of Single Silver Nanoparticles and Their Dimers, One at a Time. *J. Phys. Chem. Lett.* **2010**, *1*, 696–703. [[CrossRef](#)]
12. Wan, F.; Shi, H.; Chen, W.; Gu, Z.; Du, L.; Wang, P.; Wang, J.; Huang, Y. Charge Transfer Effect on Raman and Surface Enhanced Raman Spectroscopy of Furfural Molecules. *Nanomaterials* **2017**, *7*, 210. [[CrossRef](#)]
13. Yamamoto, Y.S.; Ozaki, Y.; Itoh, T. Recent Progress and Frontiers in the Electromagnetic Mechanism of Surface-Enhanced Raman Scattering. *J. Photochem. Photobiol. C Photochem. Rev.* **2014**, *21*, 81–104. [[CrossRef](#)]
14. Bandarenka, H.V.; Girel, K.V.; Zavatski, S.A.; Panarin, A.; Terekhov, S.N. Progress in the Development of SERS-Active Substrates Based on Metal-Coated Porous Silicon. *Materials* **2018**, *11*, 852. [[CrossRef](#)]
15. Puente, C.; Aguilar, N.P.; Gómez, I.; López, I. Morphology Effect of Photoconverted Silver Nanoparticles on the Performance of Surface-Enhanced Raman Spectroscopy Substrates. *ACS Omega* **2023**, *8*, 12630–12635. [[CrossRef](#)]
16. Yue, X.; Zheng, X.; Lv, G.; Mo, J.; Yu, X.; Liu, J.; Jia, Z.; Lv, X.; Tang, J. Synthesis of a Low-Cost, Stable, Silicon-Based SERS Substrate for Rapid, Nondestructive Biosensing. *Optik* **2019**, *192*, 162959. [[CrossRef](#)]
17. Zheng, Y.B.; Huang, T.J. Surface Plasmons of Metal Nanostructure Arrays: From Nanoengineering to Active Plasmonics. *SLAS Technol.* **2008**, *13*, 215–226. [[CrossRef](#)]
18. Jana, D.; Mandal, A.; De, G. High Raman Enhancing Shape-Tunable Ag Nanoplates in Alumina: A Reliable and Efficient SERS Technique. *ACS Appl. Mater. Interfaces* **2012**, *4*, 3330–3334. [[CrossRef](#)] [[PubMed](#)]
19. Xue, B.; Wang, D.; Zuo, J.; Kong, X.; Zhang, Y.; Liu, X.; Tu, L.; Chang, Y.; Li, C.; Wu, F.; et al. Towards High Quality Triangular Nanoprisms: Improved Synthesis, Six-Tip Based Hot Spots and Ultra-High Local Surface Plasmon Resonance Sensitivity. *Nanoscale* **2015**, *7*, 8048–8057. [[CrossRef](#)] [[PubMed](#)]

20. Sovizi, M.; Aliannezhadi, M. Localized Surface Plasmon Resonance (LSPR) of Coupled Metal Nanospheres in Longitudinal, Transverse and Three-Dimensional Coupling Configurations. *Optik* **2022**, *252*, 168518. [[CrossRef](#)]
21. Krajczewski, J.; Joubert, V.; Kudelski, A. Light-Induced Transformation of Citrate Stabilized Silver Nanoparticles: Photochemical Method of Increase of SERS Activity of Silver Colloids. *Colloids Surf. A Physicochem. Eng. Asp.* **2014**, *456*, 41–48. [[CrossRef](#)]
22. Shiohara, A.; Wang, Y.; Liz-Marzán, L.M. Recent Approaches Toward Creation of Hot Spots for SERS Detection. *J. Photochem. Photobiol. C Photochem. Rev.* **2014**, *21*, 2–25. [[CrossRef](#)]
23. Tiwari, V.S.; Oleg, T.; Darbha, G.K.; Hardy, W.; Singh, J.P.; Ray, P.C. Non-Resonance SERS Effects of Silver Colloids with Different Shapes. *Chem. Phys. Lett.* **2007**, *446*, 77–82. [[CrossRef](#)]
24. Jin, R.; Cao, Y.W.; Mirkin, C.A.; Kelly, K.L.; Schatz, G.C.; Zheng, J.G. Photoinduced Conversion of Silver Nanospheres to Nanoprisms. *Science* **2001**, *294*, 1901–1903. [[CrossRef](#)] [[PubMed](#)]
25. Nhung, N.T.H.; Dat, N.T.; Thi, C.M.; Viet, P.V. Fast and Simple Synthesis of Triangular Silver Nanoparticles under the Assistance of Light. *Colloids Surf. A Physicochem. Eng. Asp.* **2020**, *594*, 124659.
26. An, J.; Tang, B.; Ning, X.; Zhou, J.; Zhao, B.; Xu, W.; Corredor, C.; Lombardi, J.R. Photoinduced Shape Evolution: From Triangular to Hexagonal Silver Nanoplates. *J. Phys. Chem. C* **2007**, *111*, 18055–18059. [[CrossRef](#)]
27. Nguyen, V.T. Sunlight-Driven Synthesis of Silver Nanoparticles Using Pomelo Peel Extract and Antibacterial Testing. *J. Chem.* **2020**, *2022*, 6407081. [[CrossRef](#)]
28. Stamplecoskie, K.G.; Scaiano, J.C.; Tiwari, V.S.; Anis, H. Optimal Size of Silver Nanoparticles for Surface-Enhanced Raman Spectroscopy. *J. Phys. Chem. C* **2011**, *115*, 1403–1409. [[CrossRef](#)]
29. Xue, C.; Métraux, G.S.; Millstone, J.E.; Mirkin, C.A. Mechanistic Study of Photomediated Triangular Silver Nanoprism Growth. *J. Am. Chem. Soc.* **2008**, *130*, 8337–8344. [[CrossRef](#)]
30. Bartlett, T.R.; Sokolov, S.V.; Plowman, B.J.; Young, N.P.; Compton, R.G. Tracking of Photochemical Ostwald Ripening of NanoParticles Through Voltammetric Atom Counting. *Nanoscale* **2016**, *8*, 16075–16530. [[CrossRef](#)]
31. Iravani, S.; Korbekandi, H.; Mirmohammadi, S.V.; Zolfaghari, B. Synthesis of Silver Nanoparticles: Chemical, Physical and Biological Methods. *Res. Pharm. Sci.* **2014**, *9*, 385–406.
32. Chuttrakulwong, F.; Thamaphat, K.; Limsuwan, P. Photo-Irradiation Induced Green Synthesis of Highly Stable Silver NanoParticles Using Durian Rind Biomass: Effects of Light Intensity, Exposure Time and pH on Silver Nanoparticles Formation. *J. Phys. Commun.* **2020**, *4*, 095015. [[CrossRef](#)]
33. Stamplecoskie, K.G.; Scaiano, J.C. Light Emitting Diode Irradiation Can Control the Morphology and Optical Properties of Silver Nanoparticles. *J. Am. Chem. Soc.* **2010**, *132*, 1825–1827. [[CrossRef](#)]
34. Brioude, A.; Pileni, M.P. Silver Nanodisks: Optical Properties Study Using the Discrete Dipole Approximation Method. *J. Phys. Chem. B* **2005**, *109*, 23371–23377. [[CrossRef](#)]
35. Saade, J.; Araújo, C.B. Synthesis of Silver Nanoprisms: A Photochemical Approach Using Light Emission Diodes. *Mater. Chem. Phys.* **2014**, *148*, 1184–1193. [[CrossRef](#)]
36. Métraux, G.S.; Mirkin, G.A. Rapid Thermal Synthesis of Silver Nanoprisms with Chemically Tailorable Thickness. *Adv. Mater.* **2005**, *17*, 412–415. [[CrossRef](#)]
37. Wang, H.; Cui, X.; Guan, W.; Zheng, X.; Zhao, H.; Wang, Z.; Wang, Q.; Xue, T.; Liu, C.; Singh, D.J.; et al. Kinetic Effects in the Photomediated Synthesis of Silver Nanodecahedra and Nanoprisms: Combined Effect of Wavelength and Temperature. *Nanoscale* **2014**, *6*, 7295–7302. [[CrossRef](#)] [[PubMed](#)]
38. Pisárčik, M.; Lukáč, M.; Jampilek, J.; Bilka, F.; Bilková, A.; Pašková, L.; Devínsky, F.; Horáková, R.; Březina, M.; Opravil, T. Silver Nanoparticles Stabilized with Phosphorus-Containing Heterocyclic Surfactants: Synthesis, Physico-Chemical Properties, and Biological Activity Determination. *Nanomaterials* **2021**, *11*, 1883. [[CrossRef](#)] [[PubMed](#)]
39. Watanabe, H.; Hayazawa, N.; Inouye, Y.; Kawata, S. DFT Vibrational Calculations of Rhodamine 6G Adsorbed on Silver: Analysis of Tip-Enhanced Raman Spectroscopy. *J. Phys. Chem. B* **2005**, *109*, 5012–5020. [[CrossRef](#)] [[PubMed](#)]
40. Hildebrandt, P.; Stockburger, M. Surface-Enhanced Resonance Raman Spectroscopy of Rhodamine 6G Adsorbed on Colloidal Silver. *J. Phys. Chem.* **1984**, *88*, 5935–5944. [[CrossRef](#)]
41. He, X.N.; Gao, Y.; Mahjouri-Samani, M.; Black, P.N.; Allen, J.; Mitchell, M.; Xiong, W.; Zhou, Y.S.; Jiang, L.; Lu, Y.F. Surface-Enhanced Raman Spectroscopy Using Gold-Coated Horizontally Aligned Carbon Nanotubes. *Nanotechnology* **2012**, *23*, 205702. [[CrossRef](#)] [[PubMed](#)]
42. Zhong, F.; Wu, Z.; Guo, J.; Jia, D. Porous Silicon Photonic Crystals Coated with Ag Nanoparticles as Efficient Substrates for Detecting Trace Explosives Using SERS. *Nanomaterials* **2018**, *8*, 872. [[CrossRef](#)] [[PubMed](#)]
43. Wang, R.; Yao, Y.; Shen, M.; Wang, X. Green Synthesis of Au@Ag Nanostructures through a Seed-Mediated Method and Their Application in SERS. *Colloids Surf. A Physicochem. Eng. Asp.* **2016**, *492*, 263–272. [[CrossRef](#)]
44. Kelly, K.L.; Coronado, E.; Zhao, L.L.; Schatz, G.C. The Optical Properties of Metal Nanoparticles: The Influence of Size, Shape, and Dielectric Environment. *J. Phys. Chem. B* **2003**, *107*, 668–677. [[CrossRef](#)]

Disclaimer/Publisher’s Note: The statements, opinions and data contained in all publications are solely those of the individual author(s) and contributor(s) and not of MDPI and/or the editor(s). MDPI and/or the editor(s) disclaim responsibility for any injury to people or property resulting from any ideas, methods, instructions or products referred to in the content.